Chinese Chemical Letters 36 (2025) 110101

Contents lists available at ScienceDirect

Chinese Chemical Letters

journal homepage: www.elsevier.com/locate/cclet

Unprecedented stepwise electron transfer and photocatalysis in supramolecular assembly derived hybrid single-layer two-dimensional nanosheets in water

Yan Fan[a], Jiao Tan[a], Cuijuan Zou[a], Xuliang Hu[b,*], Xing Feng[c,*], Xin-Long Ni[a,*]

[a] Key Laboratory of Chemical Biology and Traditional Chinese Medicine, Ministry of Educational of China, Key Laboratory of the Assembly and Application of Organic Functional Molecules of Hunan Province, Hunan Normal University, Changsha 410081, China
[b] Institute of interdisciplinary Studies of Hunan normal University, Changsha 410081, China
[c] Guangdong Provincial Key Laboratory of Functional Soft Condensed Matter, School of Material and Energy, Guangdong University of Technology, Guangzhou 510006, China

ARTICLE INFO

Article history:
Received 18 January 2024
Revised 26 May 2024
Accepted 6 June 2024
Available online 8 June 2024

Keywords:
Hybrid single-layer 2D materials
Host-guest recognition
Outer-surface interactions
Photocatalysis

ABSTRACT

Herein, a simple and effective outer-surface interactions assisted supramolecular hierarchical assembly has been first exploited to uniformly distribute tungstosilicic acid (TSA) inside the porous structure of cucurbit[10]uril-based single-layer 2D supramolecular-organic-frameworks (Q[10]-SOFs) in water. Importantly, the 2D Q[10]-SOFs can further serve as light harvesting antenna, achieving fast energy transfer to the embedded redox-active TSA upon photoexcitation, resulting in efficient visible light-driven selective oxidation of benzyl alcohols into the corresponding aldehydes in high yield at room temperature. Further studies revealed that the integrated of 2D Q[10]-SOFs and TSA played a key role in the catalytic process, due to the presence of a novel stepwise electron transfer route in the single-layer hybrid 2D structures.

Hybrid two-dimensional (2D) nanosheets are a class of nanomaterials that are composed of two or several components within 2D frameworks [1-3]. Unlike the well-studied 2D nanomaterials, a hybrid 2D nanosheets possessed the advantages of its individual components, and emerged as a new opportunity for 2D materials owing to their smart tailored structures and adjustable functionality. These multicomponent structures hold great potential to overcome the weaknesses of the individual counterparts and offers an intelligent way to optimize the performance for specific applications. To date, a variety of hybrid 2D micro-/nano-structures have been successfully prepared through various synthetic approaches [3]. However, the investigation on ultrathin hybrid 2D nanosheets with desirable structures in solution for facile operation is still difficult to realize using the most current well-developed methods, because of their high tendency toward irreversible aggregation leads to a significant loss in the advantages arising from their 2D structural features.

Macrocycle-based supramolecular organic frameworks (SOFs) are a class of periodic self-assembled structures constructed *via* non-covalent interactions [4-6]. For example, Li and co-workers reported their pioneering work on a type of cucurbit[8]uril (Q[8] or CB[8])-derived water-soluble SOFs using various molecular building blocks prepared using directional host-guest interactions in an aqueous solution [4]. Given the advantages of their stability and porosity in an aqueous solution, these Q[8]-based SOFs have been successfully exploited in drug delivery [7,8], catalysis [9-11], chiral adaptive induction [12,13], and adsorption of organic pollutants in water [14]. Meanwhile, we discovered that Q[*n*]s could be used as rigid barrel blocks to produce a series of Q[*n*]-based solid SOFs utilizing the outer-surface interactions of Q[*n*]s [15-19]. Although the outer-surface interactions of Q[*n*]s with anionic species have been fully studied in the solid-phase, their binding behaviors in solution have been rarely studied. From a structural viewpoint, the nanocage-like Q[*n*] host derived 2D SOFs are an ideal framework to fabricate stable hybrid single-layer 2D nanosheets in water by noncovalent interactions.

In this work, a novel Q[10]-based stable single-layer 2D SOFs was constructed *via* host-stabilized charge-transfer (HSCT) interactions in water (Q[10]-SOFs) as a proof of concept study (Scheme 1). Scheme 1b shows that a number of regular positive potential appended rhombic quadrilateral pores were expected to be formed in the 2D SOFs due to the positive electrostatic potential of the outer-surface of Q[10] host. Subsequently, a hybrid single-layer 2D nanosheet could be constructed upon the addition of

* Corresponding authors.
E-mail addresses: huxuliang@hunnu.edu.cn (X. Hu), hyxhn@sina.com (X. Feng), longni333@163.com (X.-L. Ni).

https://doi.org/10.1016/j.cclet.2024.110101
1001-8417/

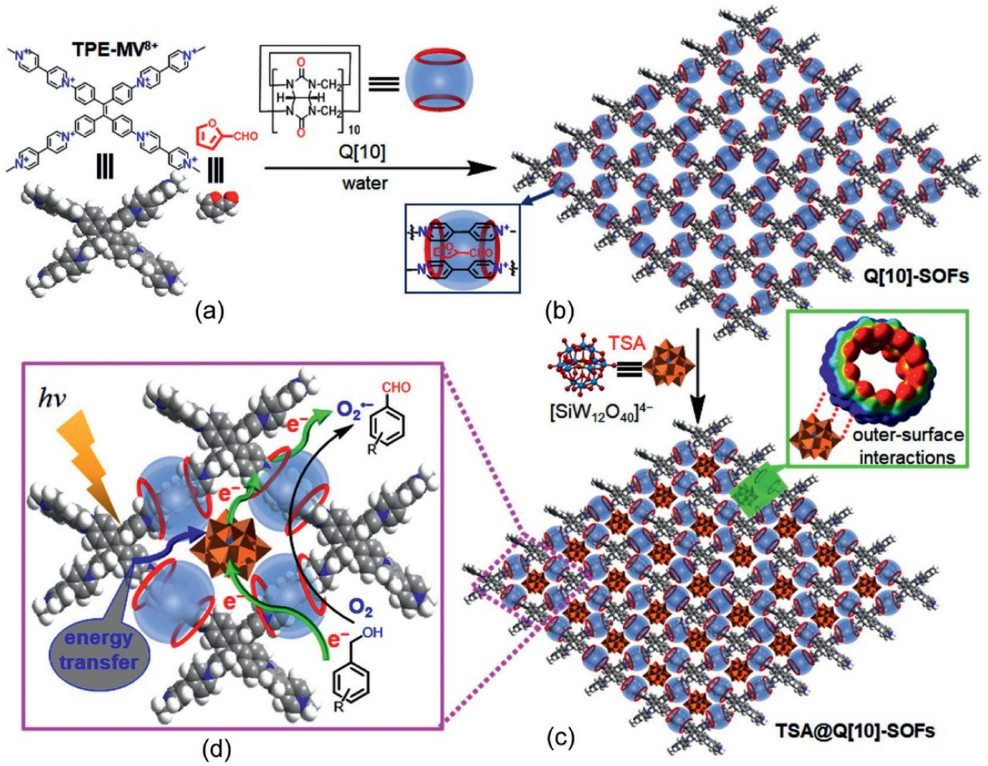

Scheme 1. (a) Chemical structures of TPE-MV^{8+}, 2-furaldehyde and Q[10]. (b) Supramolecular assembly of Q[10]-SOFs. (c) Outer-surface interactions derived assembly of TSA@Q[10]-SOFs. (d) A schematic illustration of the TSA@Q[10]-SOFs assembly engaged selective oxidation of benzyl alcohols using energy transfer and electron transfer under light irradiation.

negative charge appended tungstosilicic acid (TSA) to the Q[10]-SOFs solution *via* the outer surface interactions of the Q[10] host (Scheme 1c). Most importantly, the resulting hybrid single-layer 2D nanosheet (TSA@Q[10]-SOFs) enabled the light harvesting efficiency of TSA to be utilized [20], where the Q[10]-SOFs act as the light harvesting antenna (Scheme 1d), leading to the TSA@Q[10]-SOFs assembly being used as a catalyst for the selective photocatalytic conversion of benzyl alcohols to aldehydes in high yield in an aqueous solution at room temperature.

Q[10] has the largest nanocage size in the Q[*n*] family, and is unique due to its ability to simultaneously bind two mono-bipyridinium guest molecules (*e.g.*, methyl viologen, MV^{2+}) and an electron-rich guest molecule (*e.g.*, dihydroxynaphthalene) in its hydrophobic cavity to form a stable 2:1 inclusion complex [21]. Although Q[10] has similar guest binding behaviors to the Q[8] host, the exploration of Q[10] as molecular handcuffs to accommodate guest molecules in its cavity to form SOFs in solution has not yet been reported to date. In this work, a tetraphenylethylene supported bipyridinium guest (TPE-MV^{8+}; Cl^- as counter anions) was synthesized (Figs. S1 and S2 in Supporting information), which exhibited excellent solubility in water. Herein, the MV^{2+} group of TPE-MV^{8+} acting as an electron acceptor and the 2-furaldehyde molecule acting as an electron donor were simultaneously encapsulated into the Q[10] cavity to form single-layer 2D SOFs (Scheme 1).

^{1}H NMR spectroscopic analysis (Fig. 1) revealed that all of the proton peaks corresponding to the 2-furaldehyde molecule and H_a and H_b protons on the TPE-MV^{8+} guest molecule underwent a remarkable upfield shift, whereas the proton peaks including H_c, H_d, H_e, H_f and H_g were shifted downfield when 2.0 equiv. of Q[10] (1.0 mmol/L) was added to the mixture solution of TPE-MV^{8+} (0.5 mmol/L) and 2-furaldehyde (1.0 mmol/L) (Fig. 1c). These spectral changes suggested that the whole of the 2-furaldehyde

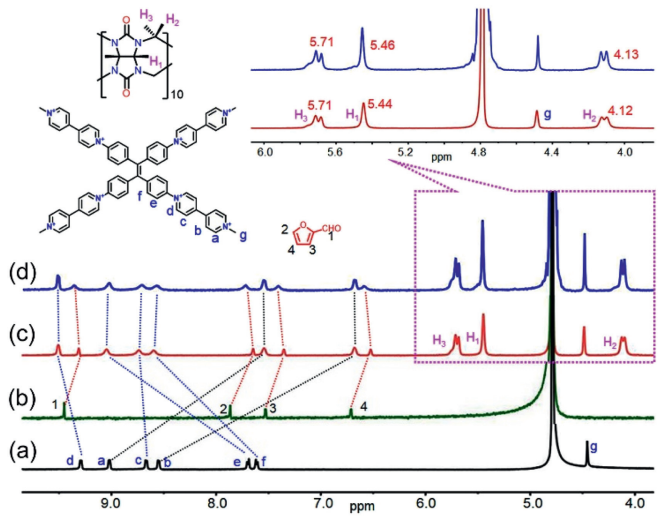

Fig. 1. ^{1}H NMR spectra obtained for (a) TPE-MV^{8+}, (b) 2-furaldehyde, (c) Q[10]-SOFs and (d) TSA@Q[10]-SOFs in D_2O.

molecules and the part of the viologen moiety in the TPE-MV^{8+} guest molecule were encapsulated in the Q[10] cavity. The corresponding COSY 2D NMR spectra obtained for the host-guest complex showed correlations between the 2-furaldehyde protons and protons H_a, H_b, H_c and H_d on the viologen moieties (Figs. S3 and S4 in Supporting information). These inter-molecular correlations suggested that the 2-furaldehyde molecule in the complex should be close to the viologen moiety, *i.e.*, a sandwich-like ternary assembly was formed in the Q[10] cavity. Dynamic light scattering (DLS) experiments revealed that the average hydrodynamic diameter of

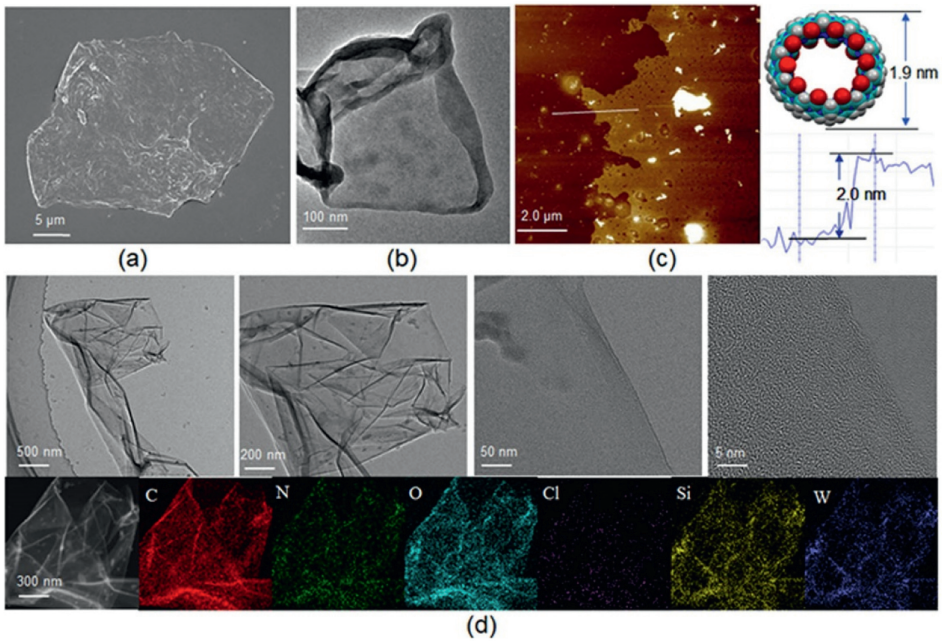

Fig. 2. (a) SEM, (b) TEM, and (c) AFM images of the Q[10]-SOFs upon slowly evaporating the aqueous solution. (d) TEM images of TSA@Q[10]-SOFs with different scale bars and the corresponding energy dispersive X-ray spectroscopy (EDS) elemental mapping images.

the host-guest assembly in water was as high as 295 nm, indicating the existence of supramolecular polymers (Fig. S5 in Supporting information). Scanning electron microscopy (SEM) and transmission electron microscopy (TEM) images showed that the 2:2:1 (mole ratio) mixture of Q[10], 2-furaldehyde and TPE-MV^{8+} gave rise to thicker planar flakes and layered films on the surfaces, respectively (Figs. 2a and b). In particular, atomic force microscopy (AFM) studies further showed the planar assemblies have a height of ~2.0 nm, in line with the height of the Q[10] host (Fig. 2c). This result strongly supported that Q[10], 2-furaldehyde and TPE-MV^{8+} formed a single-layer 2D SOFs in solution.

Polyoxometalates (POMs) are composed of large metal oxide clusters and generally present a wide range of negative charge appended anion forms in normal media. Previous studies have revealed that these anionic POMs form strong hydrogen bonding and ion-dipole interactions with the outer-surface of Q[*n*]s in the solid state [15]. In particular, POMs are generally too large to be included in the Q[*n*] cavity as normal guest molecules. All these characteristics allow POMs to be used as ideal candidates to form exclusion complexes with Q[*n*]s. Herein, it was found that TSA (an important member of the POMS family with a Keggin structure) had good compatibility with Q[10]-SOFs in aqueous media. Fig. 1d shows that upon the addition of TSA (0.5 mmol/L) to the solution of Q[10]-SOFs, no significant changes in the ^{1}H NMR spectra were observed for the protons on the TPE-MV^{8+} and 2-furaldehyde molecule, apart from the proton signals on the Q[10] host where the proton peaks undergo a slight downfield shift. This result implied the formation of an exclusion complex between the Q[10] host and TSA *via* the outer-surface interactions of Q[10] because the Q[*n*] protons were barely affected by the formation of the inclusion complex [22,23]. DLS measurements showing a diameter of 220 nm existed in the TSA@Q[10]-SOFs solution (Fig. S5 in Supporting information), indicating that the assembly of Q[10]-SOFs was retained in the presence of TSA.

TEM images of the solution of TSA@Q[10]-SOFs demonstrated that the hybrid assembly also formed film-like structures with lateral sizes of around several hundred nanometers and part of them were obviously wrinkled (Fig. 2d). Notability, the films displayed very low contrast to the carbon film-coated TEM grid, suggesting the formation of extremely thin 2D nanosheets. Most importantly, elemental mapping analysis of energy-dispersive X-ray spectroscopy (EDS) showed that C, N, O, Cl, Si and W were uniformly distributed in the films, which implies that TSA was uniformly dispersed in the pores of the Q[10]-SOFs (Fig. 2d). Therefore, these results provided unequivocal proof for the formation of hybrid single-layer 2D nanosheets by the supramolecular assembly of TSA and Q[10]-SOFs.

The photophysical properties of Q[10]-SOFs and the as-prepared hybrid 2D SOFs were then investigated. Fig. S6a (Supporting information) shows the UV–vis absorption of TPE-MV^{8+} in water exhibits absorbance maxima at 285 and 372 nm, which belong to the π-π transition of the MV^{2+} and TPE units, respectively. The absorbance intensity observed at a shorter wavelength was significantly enhanced and exhibits a red-shift at the longer wavelength after the addition of Q[10] and 2-furaldehyde to the solution, which can be attributed to the HSCT interactions formed between the MV^{2+} and 2-furaldehyde moieties, indicating the formation of Q[10]-SOFs. The continued addition of TSA to the Q[10]-SOFs solution caused a stronger absorption at 285 nm and a further red-shift of the longer wavelength of TPE-MV^{8+} to the visible-light region. Essentially, the UV–vis absorption with further red-shift was ascribed to the formation of a more rigid planar 2D structure of the SOFs after embedding TSA into the framework, which enhances the charge transfer between of 2-furaldehyde and MV^{2+} groups in the Q[10] cavity. For comparison, the UV–vis absorption peaks of the free TSA and 2-furaldehyde molecules exhibit a weaker intensity at 270 and 291 nm under the same experiment conditions, respectively. These UV–vis absorption properties suggested that the Q[10]-SOFs acted as a light harvesting antenna and may be favorable for the collection and transfer of energy from visible light to the TSA moiety in an aqueous solution.

POMs are attractive candidates for catalysis due to their ability to undergo fast, reversible, and multiple electron transfer reactions, but their applications have been hindered by several drawbacks, such as their poor visible-light utilization efficiency and self-aggregation in solution. Although various modification methods,

including heteroatom doping, transition-metal-substituted, MOF- and COF-junctions have been developed to improve the visible light harvesting ability and catalytic activity of POMs [24], there are few reports on POM-2DSOFs. As shown in Fig. S6b (Supporting information), after incorporation of TSA into the Q[10]-SOFs, the solid-state UV diffuse reflectance (UV-DRS) spectra indicated that the light response of TSA distinctly strengthens in the visible light region compared to pure TSA. Based on the Tauc plot (Fig. S6c in Supporting information), the bandgap energies (E_g) of TSA, Q[10]-SOFs and TSA@Q[10]-SOFs were calculated to be 3.08, 2.16, and 2.09 eV, respectively [25]. The calculated E_g of TSA in this work is closed to the reported value of 3.26 eV [26]. The flat potential of Q[10]-SOFs and TSA@Q[10]-SOFs were determined to be −1.50 and −1.40 V as measured by Mott–Schottky plots (Figs. S6d and S7 in Supporting information), respectively. The positive slope of both structures is consistent with the typical n-type semiconductors. As a result, the conduction band (E_{CB}) positions of Q[10]-SOFs and TSA@Q[10]-SOFs were calculated to be −1.30 and −1.20 V *versus* normal hydrogen electrode (*vs.* NHE), and the corresponding position of the valance band potentials (E_{VB}) is situated at +0.86 and +0.89 V *vs.* NHE, respectively, according to the formula $E_{VB} = E_{CB} + E_g$. These results suggested the Q[10]-SOFs and TSA would retain their independent photophysical characteristics in the hybrid single-layer 2D structures. To further understand the separation efficiency of photogenerated charge carriers, transient photocurrent response curves of TSA, Q[10]-SOFs and TSA@Q[10]-SOFs were measured with several visible-light on−off cycles in a three-electrode system. As depicted in Fig. S6e (Supporting information), the photocurrent density of TSA@Q[10]-SOFs is much higher than that of TSA and Q[10]-SOFs under the same conditions, indicating a higher separation efficiency of the photogenerated electron−hole pairs was achieved in the hybrid single-layer 2D nanosheets. Moreover, the arc radius of TSA@Q[10]-SOFs in the Nyquist plot is smaller than that of TSA and Q[10]-SOFs (Fig. S6f in Supporting information), implying the smallest transfer resistance of the interface electrons over TSA@Q[10]-SOFs [27]. All of these results suggest that combining the TSA into Q[10]-SOFs by the outer-surface interactions led to superior photo-induced hole–electron separation and transport efficiency on the long-range ordered single-layer 2D structures. The higher efficiency of charge immigration and separation is more conducive to enhancement of the photocatalytic activity of TSA@Q[10]-SOFs. Subsequently, the catalytic activity of TSA@Q[10]-SOFs was exploited for the selective oxidation of benzyl alcohols into their corresponding aldehydes because of the tailored POMs can not only activate O_2 to form reactive oxygen species (ROS) under light irradiation, but also adsorb and activate alcohols in the catalytic process.

Although the application of hybrid POM-photocatalysts has been studied for the selective oxidation of benzyl alcohols to the corresponding aldehyde compounds, the moderate conversion yield of the product and the use of high-energy light sources are the main limitations of these materials [28,29]. Herein, the 4-methylbenzyl alcohol was selected as a model substrate to optimize the reaction conditions. Table 1 and Fig. S8 (Supporting information) show the TSA@Q[10]-SOFs nanosheets exhibited the highest catalytic activity to produce the desired aldehyde in the presence of O_2 in water under white LED light source (10 W, 400–830 nm) at room temperature, and the reaction was completed in 2 h with the conversion rate of 99% (entry 1); no desired product was obtained when an argon atmosphere was used instead of O_2 (entry 2), indicating that this catalytic process was an O_2-mediated oxidation reaction. Notably, a trace conversion yield of benzyl alcohol was achieved when Q[10]-SOFs (entry 3), TPE-MV^{8+} (entry 4) and TSA (entry 5) were used as the catalyst under the conditions used in entry 1, even when the reaction time was extended. These results indicated that the light energy transfer from the Q[10]-SOFs antenna to the TSA group played a crucial role in activating the catalytic effect of the hybrid 2D SOFs.

Table 1
Oxidation of 4-methylbenzyl alcohol in different catalysts under white LED light source (10 W, 400–830 nm) irradiation.

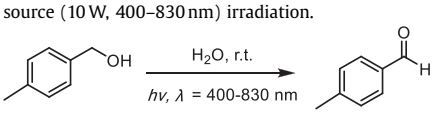

Entry	Catalyst	Time (h)	Conditions	Conversion (%)
1	TSA@Q[10]-SOFs	2	O_2	99
2	TSA@Q[10]-SOFs	10	Ar	Trace
3	Q[10]-SOFs	10	O_2	Trace
4	TPE-MV^{8+}	10	O_2	trace
5	TSA	10	O_2	trace

With the optimal reaction conditions in hand, the oxidation of various benzyl alcohols into their corresponding aldehydes over the TSA@Q[10]-SOFs was performed. Table S1 (Supporting information) shows that the photocatalysis of alcohols including electron-donating and electron-withdrawing substituents, and different positions of substituents on the aromatic ring occurs successfully to achieve their corresponding aldehydes in excellent yield (Figs. S8-S17 in Supporting information). The recycling experiments demonstrated that the catalytic activity of the hybrid 2D SOFs was well retained even after four runs of the benzyl alcohol oxidation reaction without any treatment or activation (Fig. S18 in Supporting information), indicating that the supramolecular assembly of TSA@Q[10]-SOFs as a catalyst had greater stability in water.

Encouraged by the excellent photocatalytic performance of TSA@Q[10]-SOFs in the oxidation of benzyl alcohol, we proceeded to investigate the detailed mechanism of this reaction. To clarify which active oxygen species were actually generated in this reaction system, 9,10-anthracenediyl-bis(methylene)-dimalonic acid (ABDA) and dihydroethidium (HE) as ROS indicators [30] were introduced into the reaction to specifically monitor the generation of $^1O_2$ and $O_2^{\bullet-}$, respectively. Figs. 3a and b, and Figs. S19 and S20 (Supporting information) show the decreased UV–vis absorption intensity of ABDA and enhanced fluorescence emission of HE, indicating both $^1O_2$ and $O_2^{\bullet-}$ were generated as the active species by TSA@Q[10]-SOFs after light irradiation. Meanwhile, similar spectroscopic changes for ABDA were recorded for Q[10]-SOFs and TPE-MV^{8+}, apart from TSA, where no obvious spectroscopic changes were observed for both indictors. Notability, TSA@Q[10]-SOFs exhibited the fast generation of $O_2^{\bullet-}$ when compared to Q[10]-SOFs, particularly when triethanolamine (TEOA) was added as a sacrificial electron donor to the solution (Fig. 3b). These results revealed that the integrated assembly of Q[10]-SOFs and TSA played a key role in the generations of $O_2^{\bullet-}$. Unexpectedly, additional experiments revealed that H_2O_2 and $^{\bullet}OH$ were also generated by the hybrid 2D nanoshetts under the same conditions (Figs. S21 and S22 in Supporting information). To further confirm the effect of ROS and other active species in the photocatalytic reaction system, five specific scavengers including KI, L-glutamic acid, catalase, L-ascorbic acid and D-mannitol that exclusively inhibit the generation of holes, $O_2^{\bullet-}$, H_2O_2, $^1O_2$ and $^{\bullet}OH$, respectively, were introduced into the reaction system [31], where the 4-methylbenzyl alcohol was still selected as the reaction substrate. As shown in Fig. S23 (Supporting information), no significant effect on the photocatalytic oxidation of 4-methylbenzyl alcohol in the presence of catalase and L-ascorbic acid, while the reaction yield quickly decreased with the addition of L-glutamic acid to the solution, and moderated decreased in the presence of KI and D-mannitol, respectively. These results suggested that $O_2^{\bullet-}$, holes, and $^{\bullet}OH$ participated in the reaction of benzyl alcohol, where $O_2^{\bullet-}$may as the dominant radicals.

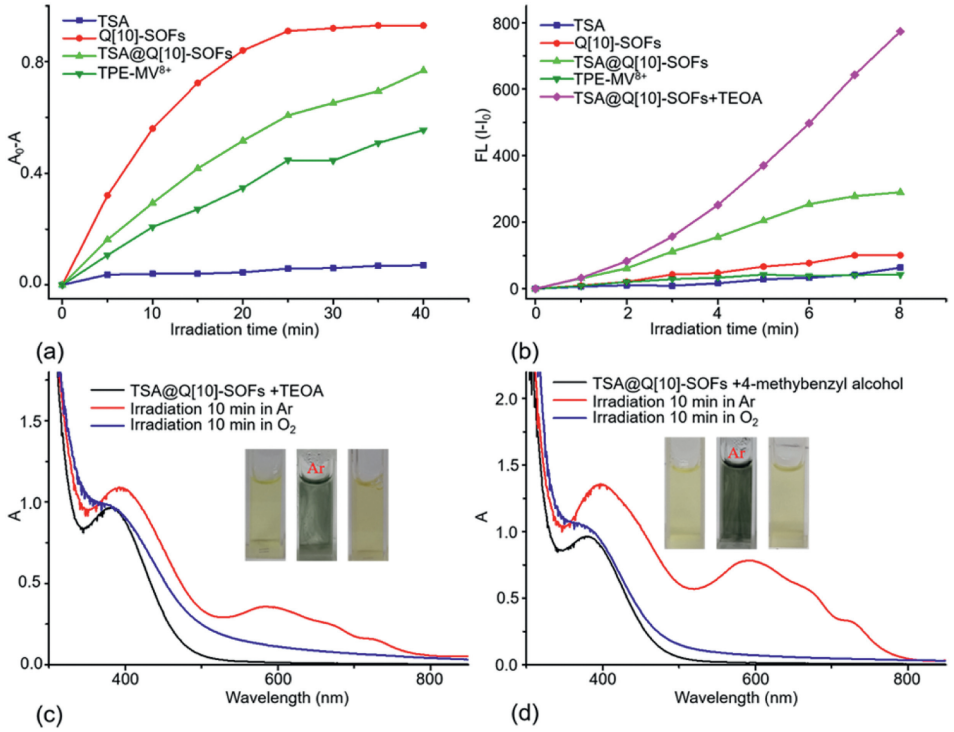

Fig. 3. Degradation rates of (a) ABDA and (b) HE using TAS, Q[10]-SOFs, TAS@Q[10]-SOFs and TPE-MV^{8+}; A_0 and A are the absorbance of ABDA, and I_0 and I are the intensity of HE in the presence of the different species before and after irradiation with white light, respectively. The UV–vis absorption spectra obtained for TSA@Q[10]-SOFs and the corresponding photographs of the aqueous solution in the presence of (c) TEOA and (d) 4-methylbenzyl alcohol before and after light irradiation under different gas atmospheres.

Interestingly, a photochromic phenomenon was further observed over TSA@Q[10]-SOFs during our evaluation of the photocatalytic mechanism. When a mixture of TSA@Q[10]-SOFs and TEOA (or benzyl alcohol) in water was irradiated with visible light under an argon atmosphere (Figs. 3c and d), the color of the solution changes from pale yellow to a cyan accompanied by a new broad absorption peak with strong intensity at 500–800 nm in the UV–vis spectrum, which indicates the formation of viologen radicals [32]. However, when O_2 was introduced into the solution, no obvious changes in the color and UV–vis absorption were observed (Figs. 3c and d), implying that the $V^{\bullet+}$ radicals can be scavenged by molecular oxygen to produce $O_2^{\bullet-}$. In addition, slight changes in the color and UV–vis absorption were observed in the solution of TSA@Q[10]-SOFs under an argon atmosphere (Fig. S24a in Supporting information), indicating the electron of $V^{\bullet+}$ radicals is mainly derived from the TSA activate alcohols rather than directly from the water molecules. On the contrary, no significant changes in the color and UV–vis absorption were triggered in the aqueous solution of Q[10]-SOFs, TPE-MV^{8+} and TSA under the same conditions (Figs. S24b-d in Supporting information), respectively. These results indicated the Q[10]-SOFs as light harvesting antenna activated TSA played a crucial role in the photocatalytic oxidation of alcohols *via* a stepwise electron transfer process.

X-ray photoelectron spectroscopy (XPS) analysis of the hybrid TSA@Q[10]-SOFs catalyst was performed to elucidate its elemental composition and valence state. Fig. S25 (Supporting information) shows the XPS spectra indicate the presence of C, N, O, Si, W and Cl in the catalyst. After light irradiation, it was clearly observed that a new peak at 400.06 eV appeared in the N 1s core-level spectrum (Fig. S26a in Supporting information), which was assigned to the nitrogen atom of the pyridyl radical on the viologen moieties [33]. Meanwhile, two new peaks at 34.86 and 37.31 eV were observed in the W 4f core-level spectrum, indicating the high-valence W^{6+} was partially reduced to W^{5+} (Fig. S26b in Supporting information) [34]. On the other hand, the C 1s and Cl 2p core-level spectra suggested that the binding energy of C=N^+ (in the V^{2+} moieties) and the Cl^- counter anion shifted from 284.72 to 197.88 eV to the higher energy level of 284.95 and 198.24 eV (Figs. S26c and d in Supporting information), respectively, indicating both atoms acted as electron donors in the hybrid 2DSOFs. As for Si 2p and O 1s, no obvious binding energy changes were observed in their core-level spectra upon irradiation with light (Fig. S27 in Supporting information). These spectroscopic changes implied that the MV^{2+} moieties and TSA in the TSA@Q[10]-SOFs nanosheets have an excellent electron acceptor ability, where the counter anions, water, and benzyl alcohols acted as electron donors.

Based on the results of above studies, a plausible mechanism for the as-prepared TSA@Q[10]-SOFs selective photocatalytic oxidation of benzyl alcohol to produce its corresponding aldehyde was proposed. As shown in Fig. 4a, the conduction band (CBs) of Q[10]-SOFs and TSA are −1.30 and 0.04 V (*vs.* NHE), and the valance band (VBs) were calculated to be 0.86 and 3.26 V (*vs.* NHE), respectively. Obviously, the CB position of Q[10]-SOFs lower than 0.33 V ($E(O_2/O_2^{\bullet-}) = -0.33$ V *vs.* NHE), 0.68 V ($E(O_2/H_2O_2) = 0.68$ V *vs.* NHE) and 1.07 V ($E(H_2O_2/^{\bullet}OH) = 1.07$ V *vs.* NHE) [29], indicating the potential of reducing O_2 into $O_2^{\bullet-}$, H_2O_2 and $^{\bullet}OH$. However, the CB position of TSA is higher than $E(O_2/O_2^{\bullet-})$ and lower than $E(O_2/H_2O_2)$ and $E(H_2O_2/^{\bullet}OH)$, suggested that TSA did not have the ability to activate O_2 into $O_2^{\bullet-}$, but can activate O_2 into H_2O_2 and $^{\bullet}OH$. In the meantime, it was found that the CB position of TSA is lower than the VB position of Q[10]-SOFs, which means that more photogenerated electrons from TSA can effectively transfer to the V^{2+} moieties of Q[10]-SOFs and further reduce O_2 into $O_2^{\bullet-}$or other ROS. While the holes reserved in TSA enable the electron donor benzyl alcohol to be oxidized.

In other words, as shown in Fig. 4b, under light-irradiation, the light energy was first harvested by the Q[10]-SOFs, then transferred to the TSA moieties, and the electron-hole pairs of TSA

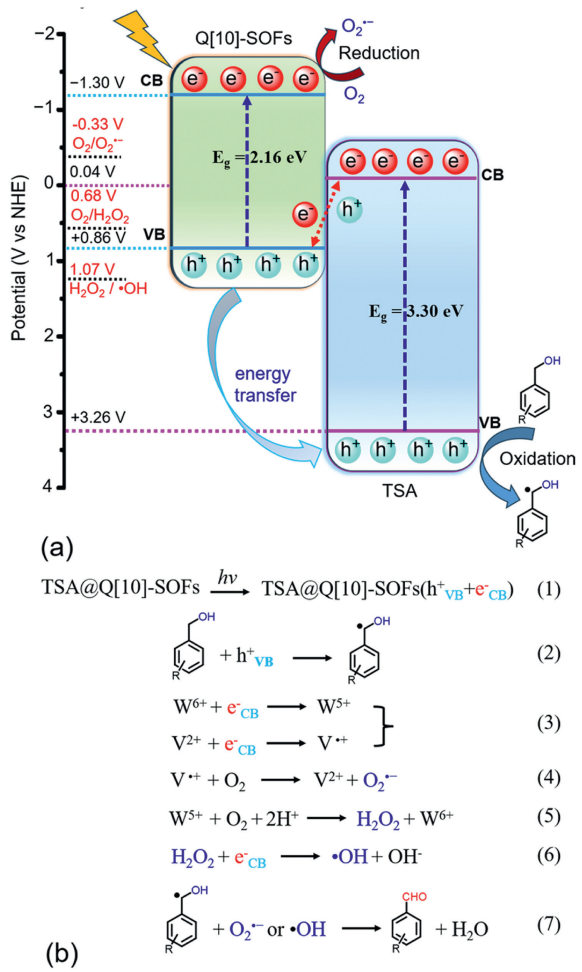

Fig. 4. (a) Schematic illustration for the energy band positions and electron transfer of the hybrid 2D materials. (b) Proposed mechanism of light energy transfer triggered ROS generation and photo-oxidation reaction in the current catalytic system.

were then generated (Eq. 1). Due to the close integration between the Q[10]-SOFs and TSA, electron transfer from the CB of the TSA species to the V^{2+} of Q[10]-SOFs was facilitated. Therefore, the electrons in the CBs of TSA were partially captured by the V^{2+} sites to form $V^{\bullet+}$ radicals and partially captured by the W^{6+} sites in TSA to form W^{5+} species (Eq. 3). Meanwhile, the electrons in both sites were more likely to be scavenged by molecular oxygen to produce $O_2^{\bullet-}$ radicals or other ROS in an O_2 atmosphere (Eqs. 4–6). Most importantly, during the light-energy-transfer-driven photo-oxidation process of benzyl alcohol, the benzyl alcohol not only acts as sacrificial electron donor to provide electrons *via* the holes on the valence band (VB) of TSA (Eq. 2), but also as activated radical intermediates that react with $O_2^{\bullet-}$ or $^{\bullet}OH$ to generate the target aldehyde (Eq. 7) and further promote the catalytic reaction cycle. Overall, the integrated of Q[10]-SOFs and activate TSA in the long-range ordered single-layer 2D structures, plays a key role in promoting the unique stepwise electron transfer process involving the optically induced hopping of electrons from benzyl alcohol to V^{2+} and W^{6+} sites in the hybrid 2DSOFs.

In summary, a simple and effective supramolecular hierarchical assembly has been exploited to prepare a tailored hybrid single-layer 2D material based on a stable host-guest interaction-derived SOFs, which uniformly distributed an earth abundant element-based TSA in its regular porous structure *via* the outer-surface interactions of the Q[10] host in water. Efficient light energy transfer between the integrated photosensitive 2D SOFs and TSA cluster occurred in the TSA@Q[10]-SOFs, leading to a unique light-driven oxidation reaction by a Keggin-type POM *via* the synergistic photoexcitation of the SOFs and stepwise electron hopping from the excited states of the TSA and activated benzyl alcohols. Furthermore, the nanocage-like macrocycle-based SOFs with a long-range ordered structure and high specific surface area ensured the uniform distribution of TSA in the single-layers, which cannot only prevent the self-aggregation of TSA, but also allowed the exposure of more active sites for catalysis in solution. The modular and tunable nature of this noncovalent interactions-derived supramolecular approach with low cost and facile operation provided an updated insight into the design of multifunctional hybrid single-layer 2D materials and their applications in solution.

Declaration of competing interest

The authors declare no competing financial interest.

Acknowledgment

This work was supported by the National Natural Science Foundation of China (No. 22271090).

Supplementary materials

Supplementary material associated with this article can be found, in the online version, at doi:10.1016/j.cclet.2024.110101.

References

[1] K. Jayaramulu, B. Devi, Chem. Mater. 35 (2023) 9473–9492.
[2] T. Yang, Y. Liu, L. Hua, et al., Chin. Chem. Lett. 35 (2024) 108707.
[3] X. Huang, C. Tan, Z. Yin, H. Zhang, Adv. Mater. 26 (2014) 2185–2204.
[4] K.D. Zhang, J. Tian, D. Hanifi, et al., J. Am. Chem. Soc. 135 (2013) 17913–17918.
[5] L. Mao, S. Li, X. Zhang, Z.T. Li, D. Ma, Chin. Chem. Lett. 34 (2023) 109363.
[6] L. Zhou, C. Yang, W. Dou, et al., Chin. Chem. Lett. 35 (2024) 108669.
[7] Z.T. Li, S.B. Yu, Y. Liu, J. Tian, D.W. Zhang, Acc. Chem. Res. 55 (2022) 2316–2325.
[8] B. Yang, X.D. Zhang, J. Li, et al., CCS Chem. 1 (2019) 156–165.
[9] W. Xu, J.Y. Chao, B. Tang, et al., Chem. Eur. J. 28 (2022) e202202200.
[10] Y. Li, C. Yan, Q. Li, L. Cao, Sci. China Chem. 65 (2022) 1279–1285.
[11] C.C. Zhang, X. Liu, Y.P. Liu, Y. Liu, Chem. Mater. 32 (2020) 8724–8732.
[12] Y. Li, Q. Li, X. Miao, et al., Angew. Chem. Int. Ed. 60 (2021) 6744–6751.
[13] C. Yan, Q. Li, X. Miao, et al., Angew. Chem. Int. Ed. 62 (2023) e202308029.
[14] J. Tian, T.Y. Zhou, S.C. Zhang, et al., Nat. Commun. 5 (2014) 5574.
[15] X.L. Ni, X. Xiao, H. Cong, et al., Acc. Chem. Res. 47 (2014) 1386–1395.
[16] X. Cui, W. Zhao, K. Chen, et al., Chem. Eur. J. 23 (2017) 2759–2763.
[17] Y.Q. Yao, Y.J. Zhang, C. Huang, et al., Chem. Mater. 29 (2017) 5468–5472.
[18] Y. Huang, R.H. Gao, M. Liu, et al., Angew. Chem. Int. Ed. 60 (2021) 15166–15191.
[19] C. Liu, Y. Xia, Z. Tao, X.L. Ni, Chin. Chem. Lett. 33 (2022) 1529–1532.
[20] Z. Wu, H. Qian, X. Li, T. Xiao, L. Wang, Chin. Chem. Lett. 35 (2024) 108829.
[21] W. Gong, X. Yang, P.Y. Zavalij, et al., Chem. Eur. J. 22 (2016) 17612–17618.
[22] W. Wang, X. Wang, J. Cao, et al., Chem. Commun. 54 (2018) 2098–2101.
[23] D. Song, B. Li, X. Li, et al., ChemSusChem 13 (2020) 394–399.
[24] M. Lu, M. Zhang, J. Liu, et al., J. Am. Chem. Soc. 144 (2022) 1861–1871.
[25] Y. Deng, L. Tang, C. Feng, et al., Appl. Catal. B: Environ. 235 (2018) 225–237.
[26] L. Chen, W.L. Chen, X.L. Wang, et al., Chem. Soc. Rev. 48 (2019) 260–284.
[27] P. Yang, H. Ou, Y. Fang, X. Wang, Angew. Chem. Int. Ed. 56 (2017) 3992–3996.
[28] X. Yang, H. Zhao, J. Feng, et al., J. Catal. 351 (2017) 59–66.
[29] D. Tang, G. Lu, Z. Shen, et al., J. Energy Chem. 77 (2023) 80–118.
[30] Y. Nosaka, A.Y. Nosaka, Chem. Rev. 117 (2017) 11302–11336.
[31] C. Ayed, J. Yin, K. Landfester, K.A.I. Zhang, Angew. Chem. Int. Ed. 62 (2023) e202216159.
[32] F. Liu, S. Chowdhury, R. Rosas, et al., Org. Lett. 23 (2021) 5283–5287.
[33] X.D. Yang, R. Zhu, J.P. Yin, et al., Chem. Eur. J. 25 (2019) 13152–13156.
[34] S.C. Huang, X.X. Xia, R.X. Fan, Z.G. Qian, Chem. Mater. 32 (2020) 1937–1945.